Journal of Engineering and Applied Sciences 3 (1): 1-6, 2008
ISSN: 1816-949X

Numerical Study of the Instability Patterns Between Counter Rotating Disks

L. Djamil
Laboratory of Energy Physics, Department of Physics,
Faculty of Science, University Mentouri, Constantine, Algeria

Abstract: The flow between counter-rotating disks for aspect ratio R/h = 7, is investigated numerically. This flow gives rise to a new instability pattern, a circular chain of vortices connected to the boundary layers trough spiral arms. The physical mechanism for this instability is elucidated: the balance between the centrifugal effects of each rotating disk results in the detachment of the boundary layer over the slower rotating disk, leading to a free shear layer in the bulk of the flow, witch becomes unstable via a Kelvin-helmholtz-type instability.

Key words: Rotating flows, flow between disks, shear instability, pentagonal patterns

INTRODUCTION

The flows above or between infinite rotating disks are known as generalized von Karman, swirling flows. They have been the subject of many studies, both fundamental and applied. The reasons for this interest are multiple. First, this is a three-dimensional flow with an exact self-similar solution which gives rise to a very rich class of instability patterns. Secondly, this is model geometry for turbomachinery, hard disk drive and geophysical flows. On the one hand, instabilities occur on the inward boundary layer over the slower rotating disk and result in axisymmetric propagating circles or spiral rolls. The latter pattern received the name of positive spirals (Gauthier *et al*., 2002), because they roll up to the center in the direction of the faster disk. These two patterns are also present in the rotor-stator flow, where they have been widely studied both numerically and experimentally. As shown by Gauthier *et al.* (2002), the counter-rotating case appears to be much richer: In addition to boundary layer instabilities, it has been recently recognized that the counter-rotating flow at high enough rotation ratio also shows free shear layer instability. In a cavity R/h = 2, at a fixed value of the Reynolds number, Lopez *et al.* (2002) first observed instability of wavenumber 4 and 5 in the counter-rotating flow, in the form of "funnel-like" vortices, that they attributed to a free shear instability. For a very different aspect ratio R/h = 20.9, Gauthier *et al.* (2002) reported a new instability pattern of wavenumber 9-11, in the form of a spiral pattern not confined to the boundary layers, but rather filling the whole gap between the disks. This pattern received the name of negative spirals, since they roll up to the center in the direction of the slower disk and suggested that a free shear layer was responsible for this instability too, raising the issue of a possible continuity with the observations of Lopez *et al.* (2002). The reason for this new instability is that the topology of the counter-rotating flow drastically changes at high enough rotation ratio, evolving towards a two-cell meridian recirculation flow with a stagnation circle on the slower disk (Fig. 1). The centrifugal flow induced by the faster disk recirculates towards the center of the slower disk due to the lateral end wall. This inward recirculation flow meets the outward radial flow induced by the slower disk, leading to a stagnation circle. The inward boundary layer on the slower disk gets detached due to this stagnation circle, leading to a free shear layer in the bulk of the flow. This free shear layer may become unstable, leading to an azimuthal modulation and giving rise to the above mentioned funnel-like vortices (Lopez *et al*., 2002) or negative spirals (Gauthier *et al*., 2002).

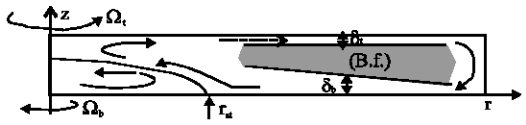

Fig. 1: Sketch of the flow in the meridian plane in the counter-rotation flow (Moisy *et al*., 2003)

In the present study, we report new observations of the instability patterns in the counter-rotating flow by numerical simulation of an incompressible viscous fluid flow between two counter-rotating disks, where the aspect ratio R/h = 7 and the Reynolds number associated to the top disk is Re_t =282 and the Reynolds number associated to the bottom disk is Re_b = 51.8 (These parameters are selected to allow the comparison between our results and those of Moisy *et al*., 2003).

MATHEMATICAL MODEL

We consider an incompressible viscous fluid flow between two parallel rotating disks enclosed by a cylindrical envelope attached to the upper disk. The upper disk and the lateral endwall are in rotation with the same angular velocity Ω_t. The bottom disk turns in the opposite direction with the angular velocity Ω_b (Fig. 2).

The three-dimensional flow between two rotating disks is modeled by the mass and impulsion conservation equations, in the cylindrical coordinates according to the 3 directions radially, azimuthally and axially.

Equation of continuity:

$$\frac{1}{r}\frac{\partial}{\partial r}(r\cdot u)+\frac{1}{r}\frac{\partial w}{\partial \theta}+\frac{\partial v}{\partial z}=0 \quad (1)$$

Equation of momentum in the radial direction:

$$\rho\left[\frac{\partial u}{\partial \tau}+\frac{1}{r}\frac{\partial}{\partial r}(ru.u)+\frac{1}{r}\frac{\partial}{\partial \theta}(w.u)+\frac{\partial}{\partial z}(v.u)\right]= \mu\left[\frac{1}{r}\frac{\partial}{\partial r}\left(r\frac{\partial u}{\partial r}\right)+\frac{1}{r}\frac{\partial}{\partial \theta}\left(\frac{1}{r}\frac{\partial u}{\partial \theta}\right)+\frac{\partial}{\partial z}\left(\frac{\partial u}{\partial z}\right)\right]-\frac{\partial p}{\partial r} -\left[\mu\left(\frac{u}{r^2}+\frac{2}{r^2}\frac{\partial w}{\partial \theta}\right)-\rho\frac{w^2}{r}\right] \quad (2)$$

Equation of momentum in the azimuthally direction:

$$\rho\left[\frac{\partial w}{\partial \tau}+\frac{1}{r}\frac{\partial}{\partial r}(rw.u)+\frac{1}{r}\frac{\partial}{\partial \theta}(w.w)+\frac{\partial}{\partial z}(w.v)+\frac{w.u}{r}\right] =\mu\left[\frac{1}{r}\frac{\partial}{\partial r}\left(r\frac{\partial w}{\partial r}\right)+\frac{1}{r}\frac{\partial}{\partial \theta}\left(\frac{1}{r}\frac{\partial w}{\partial \theta}\right)+\frac{\partial}{\partial z}\left(\frac{\partial w}{\partial z}\right)\right]-\frac{1}{r}\frac{\partial p}{\partial \theta} -\left[\mu\left(\frac{w}{r^2}-\frac{2}{r^2}\frac{\partial u}{\partial \theta}\right)-\rho\frac{wu}{r}\right] \quad (3)$$

Equation of momentum in the axial direction:

$$\rho\left[\frac{\partial v}{\partial \tau}+\frac{1}{r}\frac{\partial}{\partial r}(rv.u)+\frac{1}{r}\frac{\partial}{\partial \theta}(v.w)+\frac{\partial}{\partial z}(v.v)\right] =\mu\left[\frac{1}{r}\frac{\partial}{\partial r}\left(r\frac{\partial v}{\partial r}\right)+\frac{1}{r}\frac{\partial}{\partial \theta}\left(\frac{1}{r}\frac{\partial v}{\partial \theta}\right)+\frac{\partial}{\partial z}\left(\frac{\partial v}{\partial z}\right)\right]-\frac{\partial p}{\partial z} \quad (4)$$

Initial condition:

At $\tau = 0$:

$$u(r,\theta,z)=v(r,\theta,z)=w(r,\theta,z)=0 \quad (5)$$

Boundary conditions: The boundary conditions of the problem are expressed by:

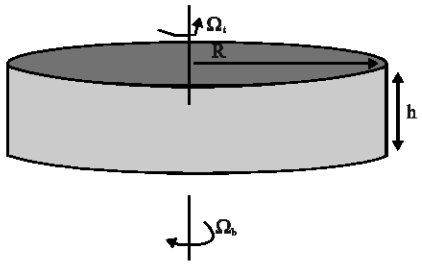

Fig. 2: Set-up scheme

Condition of the rotation of the disks:

$$\text{At. } z = 0, u = v = 0, w = r\,\Omega_b \quad (6)$$

$$\text{At. } z = h, u = v = 0, w = r\,\Omega_t \quad (7)$$

Condition of the periodicity:

$$\begin{aligned} u(r,\theta,z) &= u(r,\theta,+2\pi,z)\\ v(r,\theta,z) &= v(r,\theta,+2\pi,z)\\ w(r,\theta,z) &= w(r,\theta,+2\pi,z)\end{aligned} \quad (8)$$

The dynamic condition on the cylinder axis:

$$\frac{\partial^2 u}{\partial r^2}=\frac{\partial^2 v}{\partial r^2}=\frac{\partial^2 w}{\partial r^2}=0 \quad (9)$$

The flow is characterized by three dimensionless numbers:

- The Reynolds number based on the top disk velocity $Re_t = \Omega_t h^2/\nu$.
- The Rossby number $G = \Omega_b/\Omega_t$.
- The aspect ratio $\Gamma = R/h$.

Another parameter related to the first is the Reynolds number based on the bottom disk velocity:

$$Re_b = \Omega_b h^2 / \nu = G\ Re_t$$

In our study, we fixed the aspect ratio $\Gamma = 7$, the Reynolds number based on the top disk velocity $Re_t = 282$ (Moisy *et al.*, 2003) and the Rossby number $G = -0.184$. The variation of this last is related to the variation of the Reynolds number based on the bottom disk angular velocity Re_b.

NUMERICAL METHODS

To solve the system of non linear differential equations, we use the finite volume method described in Patankar (1980) in second order in space and time.

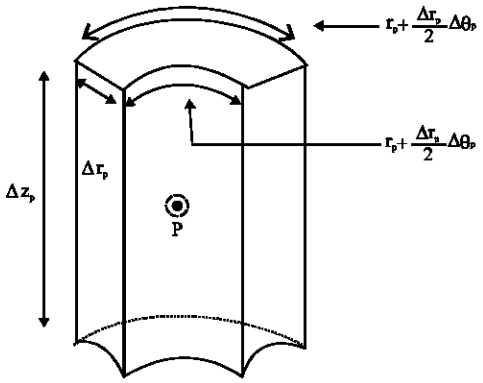

Fig. 3: Typical control volume

Spatial discretization: The physical field is transformed into a field of calculation by its division in a certain number of small cylindrical volumes. In our study, we divide the physical field into 64*32*32 finished volumes. This choice is limited by our means of calculations. Dimensions of a typical finished volume are:

$$\Delta r_p, \Delta\theta_p \text{ et } \Delta z_p$$

The Fig. 3 represents an example of cylindrical finished volume. The values of the physical quantities are stored in the typical points of finished volumes; however, the components of the field velocity are stored in the faces of volumes of control.

Discretization of the differential equations

Discretization of the temporal terms: The derivatives temporal of the equations of Navier-Stocks are discretized as specified by the following equation:

$$\frac{\partial \phi}{\partial \tau} \approx \frac{3\phi^{\tau+\Delta\tau} - 4\phi^{\tau} + \phi^{\tau-\Delta\tau}}{2\Delta\tau} + O(\Delta\tau)^2 \qquad (10)$$

Discretization of the convectifs and the non-linear terms: The convectifs terms and the non-linear terms will be approached by the discretization of Adam-Bashforth:

$$\phi^{\tau+\Delta\tau} \approx 2\phi^{\tau} - \phi^{\tau-\Delta\tau} + o(\Delta\tau)^2 \qquad (11)$$

Discretization of the other terms: The diffusive terms and the gradients of pressure will be evaluated implicitly at time $\tau = \Delta\tau$.

Space discretization: The centered differences scheme is used for the space discretization with truncation of order of $(\Delta r)^2$, $(\Delta\theta)^2$ et $(\Delta z)^2$.

The discretization of equations: The discretized equations of the components of velocity and of pressure field have the following standard form:

$$A_P\phi_P^{\tau+\Delta\tau} = A_N\phi_N^{\tau+\Delta\tau} + A_S\phi_S^{\tau+\Delta\tau} + A_E\phi_E^{\tau+\Delta\tau} + A_W\phi_W^{\tau+\Delta\tau} + A_T\phi_T^{\tau+\Delta\tau} + A_B\phi_B^{\tau+\Delta\tau} + s^{\tau+\Delta\tau} \qquad (12)$$

Where: ϕ is the dependant variable

$$A_P, A_N, A_S, A_E, A_W, A_T, A_B$$

Are the coefficients and S is the source term.

The algorithm SIMPLER is used for the sequential solutions of the systems of equations of discretization.

RESULTS AND DISCUSSION

In this research, we consider the aspect ratio $\Gamma = 7$ and the Reynolds number associated to the top disk $Re_t = 282$ and the Reynolds number associated to the bottom disk $Re_b = 51.8$ and the two disks turns in opposite directions.

The Fig. 4 represents contours of the three components velocity at different heights at $\tau = 430$. The general observation of this field indicates that the flow is not axisymmetric. At mi-height, we notice a pentagonal pattern; this pattern consists of a circular chain of five vortices whose ends rolled up in spirals by advection in the boundary layers. We call these spirals negative spirals (Moisy *et al.*, 2003).

On the Fig. 5, the axial vorticity field at mid-height is represented, we find an important concentration of vorticity separating an inner and outer part; this pentagonal pattern consists on five spirals arms in the corner, therefore this instability have a wave number m = 5.

According to the Fig. 6, we find that the meridian flow consists of two cells of circulation, the right cell is generated by the rotation of the top disk, it turns clockwise while the left cell which is due to the rotation of the bottom disk and turns in the anti-clockwise direction. Between these two cells there is a shear layer. The appearance of the vortices in the same radial position confirms that an instability of the shear layer is responsible for the appearance of the vortices.

On the Fig. 7, we represent the axial vorticity at the mid- height and the azimuthally vorticity on the bottom disk according to the radial coordinate. On the bottom disk, axial velocity component is null and by consequence

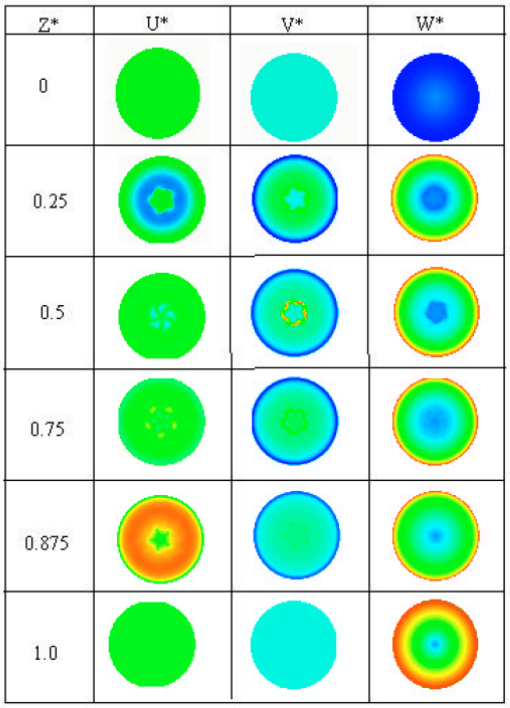

Fig. 4: Contours of the velocity field components at $\tau = 430$

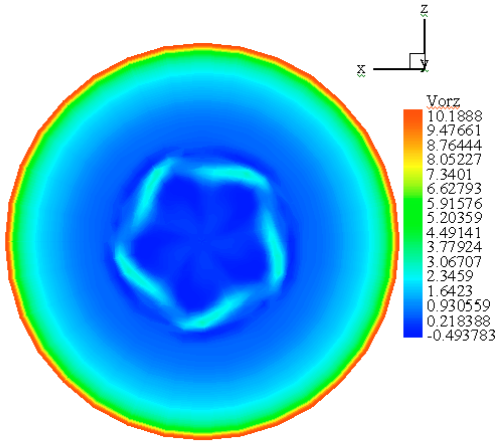

Fig. 5: Axial vorticity field at mid-height

$$\Omega_\theta = \left.\frac{\partial u}{\partial z}\right|_{z=0}$$

When it cancelled it indicates an axial gradient null of the radial velocity components. According to the Fig. 7 and it is almost the same position where the axial vorticity Ω_z is maximal. Thus, the radial position where the azimuthally vorticity is null on the bottom disc corresponds to the ray of the stagnation and the position where the axial vorticity reaches its maximum value is the ray of the shear layer. Thus, the ray of stagnation is coincided with the ray of the shear layer: $R_{St} = R_0 = 2.95$.

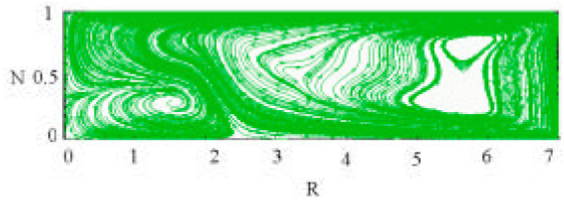

Fig. 6: Stream lines in the meridian plane, $\theta = \frac{2\pi}{5}$ at $\tau = 430$

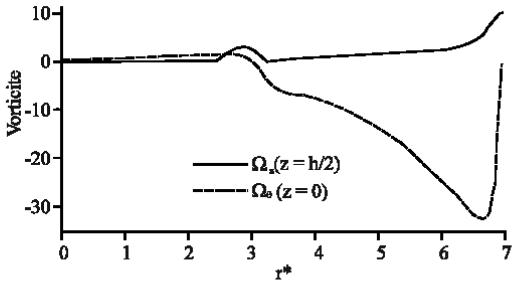

Fig. 7: The azimuthally vorticity on the bottom disk and the axial vorticity at the mid- height

The evolution of the flow in time is represented by the fields of the axial vorticity at τ = 10, 30, 40, 45, 55, 65, 70, 80, 90 on the Fig. 8. At the beginning, we find that the flow is axisymmetric until τ = 30, it is about a crown of strong vorticity in the center which it has a decreasing ray by increasing time, the value of the vorticity of this area is $\Omega_z \approx 4.34$ at τ = 10 and $\Omega_z \approx 3.50$ at τ = 30. From τ = 40, the flow becomes asymmetrical and the central area of strong vorticity starts to have an azimuthally modulations. The Fig. 8 c-g show the stages of the formation of the pentagonal pattern, therefore: The shear layer starts to become unstable from τ = 40. From τ = 80, the pattern is achieved and the flow remains with this structure for τ = 90 and τ = 95.

Figure 9 represents the temporal evolution of the radial velocity U for Re_i = 282 and Re_b = 51.8. The code computer is carried out for Re_i = 282 and G = -0.184 with a step of the time $\Delta\tau = 10^{-3}$, from 0 until τ = 230; then, we decrease the step with $\Delta\tau = 2.5*10^{-4}$ from τ = 230 until τ = 300, then we decrease the step again with $\Delta\tau$ $2.5*10^{-4}$ from τ= 300 until τ = 430, that is to say 540 h in real time of calculation. According to the Fig. 10, witch represents the temporal evolution of the two points P_1, P_2 (the

Table 1: Coordinates of test points

Point	r*	z*	θ
P_1	0.109	1	π
P_2	1.859	0.187	π/4

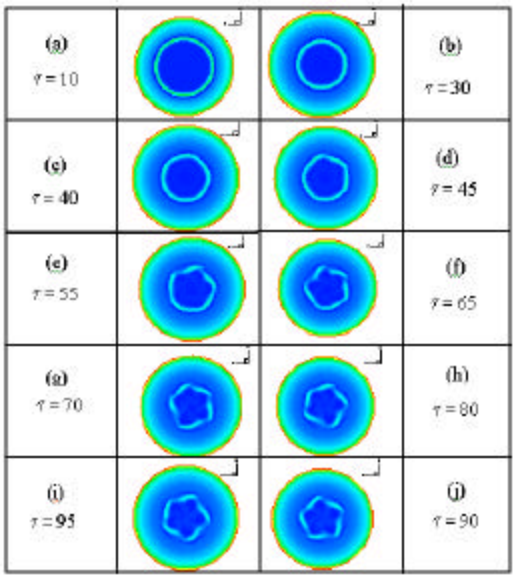

Fig. 8: Axial vorticity at mid-height

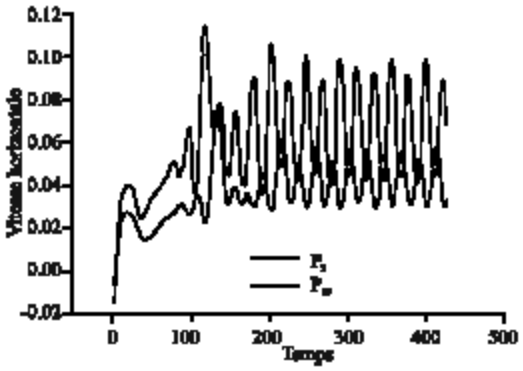

Fig. 9: Temporal evolution of the radial components velocity

coordinates of points in Table1), the flow is transitory and velocities are oscillatory. To make sure that this instability has not numerical origin, when we reduced the step of times, we found that the amplitudes of the disturbances increase further in the points of test and by consequence this instability is physical.

In order to obtain the spectrum of energy of the oscillations, we use the fast transform of Fourier (William *et al*., 1987) of a number of powers 2 of values of the temporal variation of the horizontal component velocity. In this case we use his decimal logarithm. We

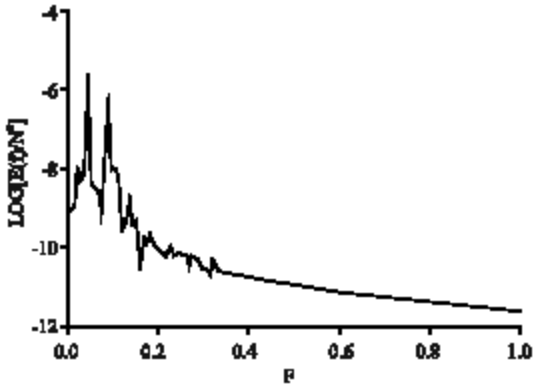

Fig. 10: Temporal spectrum of energy corresponding to the point P1

take $N = 2^{19}$, for $\Delta\tau = 2.5\times10^{-4}$, Fig. 10 illustrates the variation of the energy of the disturbances according to their frequencies at the point P_1, the dominant frequency F = 0.04578.

CONCLUSION

In this research, we study the three-dimensional flow between two rotating disks in counter rotating disks, where the Reynolds number associated to the top disk is equal to 282 and the Reynolds number associated to the bottom disk is equal to 51.8.

The problem is modeled by the equations of Navier-Stocks and continuity developed in cylindrical coordinates. These differential equations are solved by the numerical method of finite volumes in second order in space and time. The algorithm SIMPLER is used for the sequential solution of the systems of equations of discretization.

This research allowed the description of a pentagonal pattern in the center of the cylindrical enclosure, which indicates the formation of five spiral swirls which are connected by five negative spirals: A circular chain of five quasi-vertical swirls, whose ends are rolled up in spirals by advection in the boundary layers. The secondary flow in the plan (R, Z) comprises two cells of recirculation, due to the competition of the centrifugal effects associated to the rotations of the disks. This competition between the boundary layers centrifugal and centripetal on the bottom disk results a circle of stagnation where radial velocity is cancelled, causing the detachment of centripetal layer and giving rise to a annular shear layer between disks, the instability of the shear layer gives place to a pentagonal pattern with a wavenumber m = 5. The spectral analysis of a radial component velocity shows that the dominant frequency is F = 0.04578.

REFERENCES

Gauthier, G., P. Gondret, F. Moisy and M. Rabaud, 2002. Instabilities in the flow between co- and counter rotating disks. J. Fluid Mech., 473: 1-21.

Lopez, J.M., J.E. Hart, F. Marques, S. Kittelman and J. Chen, 2002. Instability and mode interactions in a differentially driven rotating cylinder. J. Fluid Mech., 462: 383-409.

Moisy, F., T. Pasutto and M. Rabaud, 2003. Instability patterns between counter rotating disks. Nonlinear Processes in Geophysics G.W. Fruh, 10: 1-8.

Patankar, S., 1980. Numerical heat transfer and fluid flow. Mc-Graw Hill, USA.

William, H. Press, Brian P. Flannery, Saul A. Teukolsky and William T. Vetterling, 1987. Numerical recipes, pp: 381-454.